Audio Engineering Society

Convention Paper

Presented at the 144th Convention
2018 May 23 – 26, Milan, Italy

Wave Digital Modeling of the Diode-Based Ring Modulator

Alberto Bernardini[1], Kurt James Werner[2], Paolo Maffezzoni[1], and Augusto Sarti[1]

[1]*Dipartimento di Elettronica, Informazione e Bioingegneria (DEIB); Politecnico di Milano, Piazza L. Da Vinci 32, 20133 Milano, Italy*
[2]*Sonic Arts Research Centre (SARC); School of Arts, English and Languages; Queen's University Belfast; 4 Cloreen Park, Belfast, BT9 5HN UK*

Correspondence should be addressed to Alberto Bernardini (alberto.bernardini@polimi.it)

ABSTRACT

The ring modulator is a strongly nonlinear circuit common in audio gear, especially as part of electronic musical instruments. In this paper, an accurate model based on Wave Digital (WD) principles is developed for implementing the ring modulator as a digital audio effect. The reference circuit is constituted of four diodes and two multi-winding transformers. The proposed WD implementation is based on the Scattering Iterative Method (SIM), recently developed for the static analysis of large nonlinear photovoltaic arrays. In this paper, SIM is shown to be suitable for implementing also audio circuits for Virtual Analog applications, such as the ring modulator, since it is stable, robust and comparable to or more efficient than state-of-the-art strategies in terms of computational cost.

1 Introduction

In this paper, Wave Digital (WD) principles will be used to make a digital model of a ring modulator circuit. Ring modulators multiply two signals (an input and a carrier) to produce an output. The basic embodiment that we will study comprises two tapped transformers, a "ring" of diodes, two sources, and a load resistor. The ring modulator was invented in 1934 by Cowan [1] and originally found use as a heterodyning element in single-sideband communications systems [2]. The carrier is often assumed to be a sine wave [3], but in theory can be any signal. Musical applications of the ring modulator were established by K. Stockhausen, the BBC Radiophonic workshop, and synthesizer manufacturers including Buchla, Moog, Oberheim, and Bode [4, 3].
Several Virtual Analog models of ring modulators exist in the literature. Hoffmann-Burchardi developed ODE descriptions of diode-based ring modulators, discretizing them directly using the forward Euler method [5]. He further studied the effects of circuit asymmetries on ring modulator behavior [6]. Parker produced a simplified and efficient model of the ring modulator by assuming a transformerless variant and making various simplifications based on the conducting arrangement of the diodes [4]. A variant of this model has been implemented by Bernardini *et al.* using WD principles [7].
In the field of digital audio signal processing, WD principles have been used for Sound Synthesis through physical modeling [8], Virtual Analog modeling [9] or the digital implementation of microphone arrays [10]. In particular, much effort has been recently devoted to the modeling of nonlinear circuits with complicated topologies [11, 12, 13] and multiple diodes [14, 15, 16, 17, 18, 7, 19, 20, 21]. An approach consisting in grouping all the nonlinearities of the circuit and then solving the nonlinear part using a multi-dimensional Newton Raphson (NR) solver has

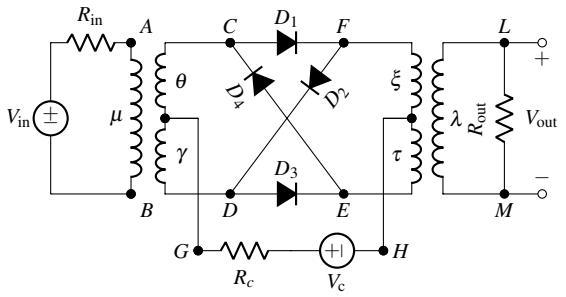

Fig. 1: Ring Modulator Schematic.

been developed in [22, 23, 24]. An alternative, even more recent, WD relaxation method for solving circuits with nonlinear two-terminal elements using one-dimensional NR solvers is introduced in [25] and employed in [26]; the method is very efficient and its convergence is theoretically guaranteed. However, the method in [25] was not used for the time domain emulation of audio circuits for Virtual Analog application, but for the static analysis of large nonlinear photovoltaic arrays. In this paper, we will show that the method in [25] can also be employed for performing very efficient and accurate time domain emulations of nonlinear audio circuits containing multiple diodes and multi-winding transformers. In particular, we will show the details of the application of this method to the ring modulator circuit in Fig. 1.

2 Modeling the connection network

N-port connection networks are realized in the WD domain using N-port junctions, characterized by $N \times N$ scattering matrices. Connection networks made of simple "wire interconnections" can be efficiently realized using the approach presented in a very useful, though semi-unknown, old article by Martens and Meerkötter [27] and recently revised in [25]. The approach in [27] was later applied to a larger class of reciprocal connection networks embedding ideal transformers [28, 29]. However, few examples of WD implementations of connection networks including ideal transformers have been discussed in the literature [28, 29, 30, 31] and, to the best of our knowledge, no examples with ideal multi-winding transformers have been published. In the first part of this Section, the formulas needed for computing the scattering matrix of a WD junction describing a reciprocal connection network are resumed, along with the fundamental properties of such a matrix. In the second part of this section, instead, we will perform an analysis of the connection network characterizing the reference circuit of the ring modulator and we will show how such a connection network containing ideal multi-winding transformers can be implemented applying the presented approach.

2.1 Theoretical background

Let us consider a N-port reciprocal connection network; $\mathbf{v} = [v_1, \ldots, v_N]^T$ and $\mathbf{j} = [j_1, \ldots, j_N]^T$ indicate the corresponding vectors of port voltages and port currents, respectively. Let us assume that $\mathbf{v}_t$ is a vector of the largest possible size q, with $1 \leq q < N$, collecting all independent port voltages, and that $\mathbf{j}_l$ is a vector of the largest possible size p, with $p = N - q$, collecting all independent port currents. As pointed out in [32], there always exists a pair of matrices $\mathbf{Q}$ and $\mathbf{B}$, having sizes $q \times N$ and $p \times N$, respectively, such that

$$\mathbf{v} = \mathbf{Q}^T \mathbf{v}_t \ , \quad \mathbf{j} = \mathbf{B}^T \mathbf{j}_l \ , \tag{1}$$

and, being the connection network reciprocal, the orthogonality property $\mathbf{B}\mathbf{Q}^T = \mathbf{0}$ holds, where $\mathbf{0}$ is a zero matrix of proper size.

Let us now consider the following definition of voltage waves [33]

$$\mathbf{a}_J = \mathbf{v} + \mathbf{Z}\mathbf{j} \ , \quad \mathbf{b}_J = \mathbf{v} - \mathbf{Z}\mathbf{j} \ , \tag{2}$$

where $\mathbf{a}_J = [a_{J1}, \ldots, a_{JN}]^T$ is the vector of waves incident to the WD junction, $\mathbf{b}_J = [b_{J1}, \ldots, b_{JN}]^T$ is the vector of waves reflected from the WD junction, while the non-zero entries of the diagonal matrix $\mathbf{Z} = \text{diag}[Z_1, \ldots, Z_N]$ are free parameters called port resistances. In the WD domain, the relation between $\mathbf{a}_J$ and $\mathbf{b}_J$ is given by

$$\mathbf{b}_J = \mathbf{S}\mathbf{a}_J \, , \tag{3}$$

where $\mathbf{S}$ is a $N \times N$ scattering matrix. Reciprocal scattering matrices are characterized by the three properties resumed in Table 1; losslessness, self-inverseness and reciprocity [27, 33, 30]. According to the results presented in [27, 28, 29], $\mathbf{S}$ can be computed according to one of the two following formulas

$$\mathbf{S} = 2\mathbf{Q}^T \left(\mathbf{Q}\mathbf{Z}^{-1}\mathbf{Q}^T\right)^{-1} \mathbf{Q}\mathbf{Z}^{-1} - \mathbf{I} \ , \tag{4}$$

$$\mathbf{S} = \mathbf{I} - 2\left(\mathbf{B}\mathbf{Z}\mathbf{B}^T\right)^{-1} \mathbf{Z}\mathbf{B}^T \ , \tag{5}$$

where $\mathbf{I}$ is the $N \times N$ identity matrix. It is evident from eq. (4) and eq. (5) that the most computationally demanding operation for the formation of $\mathbf{S}$ is the solution

Table 1: Scattering Matrix Properties

Name	Constraint
Losslessness	$\mathbf{S}^T\mathbf{Z}^{-1}\mathbf{S} = \mathbf{Z}^{-1}$
Self-inverseness	$\mathbf{S} = \mathbf{S}^{-1}$
Reciprocity	$\mathbf{S}^T\mathbf{Z}^{-1} = \mathbf{Z}^{-1}\mathbf{S}$

of a linear system. The size of such a linear system is $q \times q$, i.e. the size of matrix $\mathbf{T} = \mathbf{Q}\mathbf{Z}^{-1}\mathbf{Q}^T$, when eq. (4) is considered, or $p \times p$, i.e. the size of matrix $\mathbf{C} = \mathbf{B}\mathbf{Z}\mathbf{B}^T$, when eq. (5) is considered. It follows that, depending on whether the number of independent port voltages q is less or greater than the number of port currents p, it could be convenient to use eq. (4) or eq. (5). When $q = p$, eq. (4) and eq. (5) are basically equivalent in terms of computational cost. It is worth saying that, as explained in [25], the actual formation of $\mathbf{S}$ is not needed for computing the reflected waves and, especially dealing with large nonlinear networks, an alternative computation approach, exploiting this fact, have proved far more efficient [25]. However, when it comes to implement small nonlinear circuits, like the ring modulator in Fig. 1, such an advantage is computationally negligible.

2.2 Deriving the Ring Modulator connection network with multi-winding transformers

Let us consider the circuit in Fig. 1 and let us indicate with $V_{AB} = V_A - V_B$ the difference between the electrical potentials V_A and V_B at nodes A and B, respectively. Differences of electrical potentials between other pairs of nodes of the circuit are indicated using the same notation. The ring modulator circuit is characterized by a 7-port connection network, i.e. $N = 7$, embedding two ideal multi-winding transformers to which one resistor, two voltage sources and four diodes are connected. The connection network with the highlighted seven ports is shown in Fig. 2. Port variables are numbered and, in particular, the vector of port voltages is defined as $\mathbf{v} = [v_1, \ldots, v_7]^T$, where: $v_1 = V_{CF}$, $v_2 = V_{FD}$, $v_3 = V_{DE}$, $v_4 = V_{EC}$, $v_5 = V_{AB}$, $v_6 = V_{GH}$ and $v_7 = V_{LM}$. The ideal 3-winding transformer in the input stage is characterized by the following constraint

$$V_{AB}/\mu = V_{CG}/\theta = V_{GD}/\gamma \ , \tag{6}$$

where μ is the number of turns of the primary winding, while θ and γ are the numbers of turns of the two

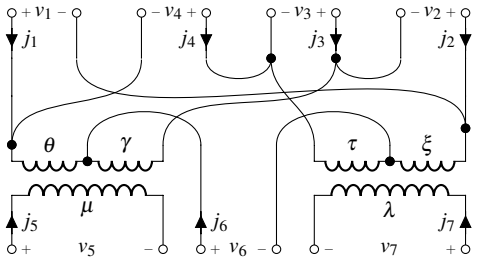

Fig. 2: Ring Modulator Connection Network.

secondary windings. Similarly, for the ideal 3-winding transformer in the output stage we have

$$V_{FH}/\xi = V_{HE}/\tau = V_{LM}/\lambda \ , \tag{7}$$

where ξ and τ are the numbers of turns of the two primary windings, while λ is the number of turns of the secondary winding. According to Kirchhoff's mesh law, we write

$$\begin{aligned} -V_{CG} + V_{CE} - V_{HE} &= V_{GH} && (8)\\ V_{GD} + V_{DE} - V_{HE} &= V_{GH} && (9)\\ -V_{CG} + V_{CF} + V_{FH} &= V_{GH} && (10)\\ V_{GD} + V_{DF} + V_{FH} &= V_{GH} \ . && (11) \end{aligned}$$

After deriving the four relations $V_{CG} = (\theta/\mu)V_{AB}$, $V_{GD} = (\gamma/\mu)V_{AB}$, $V_{FH} = (\xi/\lambda)V_{LM}$ and $V_{HE} = (\tau/\lambda)V_{LM}$ from the constraints (6) and (7) and plugging them in (8), (9), (10) and (11), we obtain the following equations, involving the port voltages,

$$\begin{aligned} v_1 &= (\theta/\mu)v_5 + v_6 - (\xi/\lambda)v_7 && (12)\\ v_2 &= (\gamma/\mu)v_5 - v_6 + (\xi/\lambda)v_7 && (13)\\ v_3 &= -(\gamma/\mu)v_5 + v_6 + (\tau/\lambda)v_7 && (14)\\ v_4 &= -(\theta/\mu)v_5 - v_6 - (\tau/\lambda)v_7 \ . && (15) \end{aligned}$$

It can be verified that we can define the vector $\mathbf{v}_t = [v_5, v_6, v_7]^T$, collecting the maximum number $q = 3$ of independent port voltages. According to (1), it is now possible to derive the following matrix

$$\mathbf{Q} = \begin{bmatrix} \theta/\mu & \gamma/\mu & -\gamma/\mu & -\theta/\mu & 1 & 0 & 0 \\ 1 & -1 & 1 & -1 & 0 & 1 & 0 \\ -\xi/\lambda & \xi/\lambda & \tau/\lambda & -\tau/\lambda & 0 & 0 & 1 \end{bmatrix} ,$$

such that $\mathbf{v} = \mathbf{Q}^T\mathbf{v}_t$. Similarly, performing an analysis based on currents, we can find a matrix

$$\mathbf{B} = \begin{bmatrix} 1 & 0 & 0 & 0 & -\theta/\mu & -1 & \xi/\lambda \\ 0 & 1 & 0 & 0 & -\gamma/\mu & 1 & -\xi/\lambda \\ 0 & 0 & 1 & 0 & \gamma/\mu & -1 & -\tau/\lambda \\ 0 & 0 & 0 & 1 & \theta/\mu & 1 & \tau/\lambda \end{bmatrix} ,$$

such that $\mathbf{j} = \mathbf{B}^T \mathbf{j}_l$, where $\mathbf{j}_l = [j_1, j_2, j_3, j_4]^T$ and $\mathbf{j} = [j_1, \ldots, j_7]^T$, hence $p = 4$. It can be verified that, as the connection network is reciprocal, $\mathbf{B}\mathbf{Q}^T = \mathbf{0}$. Since $q < p$, (4) is computationally cheaper than (5).

3 Modeling the circuit elements

In this section the constitutive equations of the used linear and nonlinear circuit elements are described. Each element is characterized by a port voltage v and a port current i, related to wave variables a and b by

$$v = (a+b)/2 \ , \quad i = (a-b)/(2Z) \ , \tag{16}$$

where Z is the reference port resistance. Starting from (16), the following useful hybrid relations are derived

$$i = (a-v)/Z \ , \tag{17}$$

$$b = 2v - a \ . \tag{18}$$

3.1 Real voltage generator and linear resistor

A real voltage generator with ideal source V_g and series resistance R_g is characterized by the constitutive equation $v = V_g + R_g i$, whose corresponding wave mapping

$$b = \frac{R_g - Z}{R_g + Z} a + \frac{2Z}{R_g + Z} V_g \tag{19}$$

reduces to $b = V_g$ when the adaptation condition $Z = R_g$ is met [33]. Similarly, a linear resistor R_g is characterized by the constitutive equation $v = R_g i$, whose corresponding wave mapping is the same of a real voltage generator (19) with $V_g = 0$ and it reduces to $b = 0$ when the adaptation condition $Z = R_g$ is met.

3.2 Diodes

An *extended Shockley diode model* is used for modeling each one of the four diodes of the ring modulator. The model is characterized by the following nonlinear constitutive equation

$$f(v,i) = I_s \left(\exp\left(\frac{v - R_s i}{\eta V_t} \right) - 1 \right) + \frac{v - R_s i}{R_p} - i = 0 \tag{20}$$

where I_s is the saturation current, η is the ideality factor, V_t is the thermal voltage, while R_s and R_p are the series resistance and the shunt resistance of the p-n junction, respectively. An explicit WD realization of (20) can be derived using the approach presented in [7], based on the Lambert function, or the approach presented in [20], based on a canonical piecewise-linear representation of nonlinear curves. However, in this article, an alternative implementation, based on a one-dimensional NR solver, is considered. Plugging (17) into (20), we get

$$h(v) = I_s \left(\exp\left(\frac{v(Z+R_s) - aR_s}{\eta V_t Z} \right) - 1 \right) + + \frac{v(Z+R_p+R_s) - a(R_p+R_s)}{ZR_p} \ ,$$

and its derivative w.r.t. v in closed-form

$$h'(v) = \frac{\partial h(v)}{\partial v} = = \frac{I_s(Z+R_s)}{\eta V_t Z} \exp\left(\frac{v(Z+R_s) - aR_s}{\eta V_t Z} \right) + \frac{Z+R_p+R_s}{ZR_p}.$$

Given the parameters of the extended Shockley diode model, the port resistance Z and the incident wave a, the port voltage v is found solving the nonlinear equation $h(v) = 0$, using an iterative NR solver based on the following updating rule

$$v^{(\iota)} = v^{(\iota-1)} - \frac{h(v^{(\iota-1)})}{h'(v^{(\iota-1)})} \ , \tag{21}$$

where the superscript between brackets is the iteration index and $\iota \geq 1$. Once the converge condition $|v^{(\iota)} - v^{(\iota-1)}| < \varepsilon_{\mathrm{NR}}$, with $\varepsilon_{\mathrm{NR}}$ a small tolerance (e.g. $\varepsilon_{\mathrm{NR}} = 10^{-10}$), is met, the NR solver is stopped and the port voltage is set to $v = v^{(\iota)}$, such that the reflected wave b can be computed, using (18). It is worth saying that, as we are dealing with a one-dimensional exponential nonlinearity, reasonable bounds on the values of v can be easily enforced such that the robustness of the NR solver is ensured, avoiding undesired overflows or divergences.

4 Scattering Iterative Method

In this Section the Scattering Iterative Method (SIM), introduced in [25] for computing the operating point of large nonlinear photovoltaic arrays, is shown to be suitable for the time domain emulation of the ring modulator. SIM can be interpreted as an iterative relaxation method and, when applied to the ring modulator, its convergence is always theoretically guaranteed. The WD structure implementing the ring modulator circuit and composed of a 7-port junction called $\mathscr{R}_1$ and seven WD elements is shown in Fig. 3.

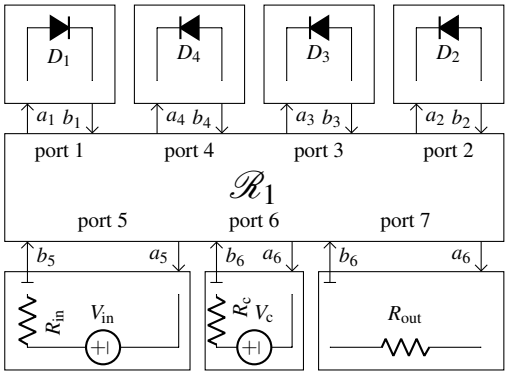

Fig. 3: WD structure implementing the ring modulator.

4.1 Computing the operating point

SIM is applied at each sampling step m of the time domain simulation for computing the operating point at each port of the circuit. $\mathbf{a}$ is the vector of waves incident to the elements and reflected from the WD junction representing the connection network, while $\mathbf{b}$ is the vector of waves reflected from the elements and incident to the junction. Vectors of port variables $\mathbf{v}$ and $\mathbf{i}$ are related to $\mathbf{a}$ and $\mathbf{b}$, according to the transformation (16). It follows that vector $\mathbf{v}$ is the same defined in Section 2, while $\mathbf{i} = -\mathbf{j}$, $\mathbf{a} = \mathbf{b}_J$ and $\mathbf{b} = \mathbf{a}_J$. Moreover, the values of port variables $\mathbf{a}$, $\mathbf{b}$, $\mathbf{v}$, $\mathbf{i}$, and the generators, V_{in} and V_{c}, are referred to the same sampling step m. SIM consists of the following four stages.

1) Initialization: each free parameter, $Z_1, \ldots, Z_N$, is set as close as possible to the slope of the line, which is tangent to the $v-i$ characteristic of the nth element and passes through the operating point at sampling step m, according to the considerations presented in Subsection 4.2. Vectors $\mathbf{a}$ and $\mathbf{v}$ are set to initial guesses $\mathbf{a}^{(0)}$ and $\mathbf{v}^{(0)}$, respectively. Usually, $\mathbf{a}$ and $\mathbf{v}$ computed at the previous sampling step $m-1$ are good initial guesses.

2) Local Scattering Stage: the wave b_n reflected from the nth element, according to (18), is given by

$$b_n^{(k)} = 2v_n^{(k)} - a_n^{(k-1)} \ , \tag{22}$$

where $1 \leq n \leq N$, the superscript between brackets is the iteration index of SIM and $k \geq 1$. The port voltage across the nth element at iteration k, $v_n^{(k)}$, is computed in a different way according to the considered WD element. In particular, in the case of the ring modulator, the port voltages across the four diodes $v_1^{(k)}$, $v_2^{(k)}$, $v_3^{(k)}$ and $v_4^{(k)}$ are returned by four separated NR solvers. The initial guesses of the NR solvers are set as $v_n^{(k-1)}$. The port voltages across the input and carrier real voltage generators are given by $v_5^{(k)} = (V_{\text{c}} + a_5^{(k-1)})/2$ and $v_6^{(k)} = (V_{\text{in}} + a_6^{(k-1)})/2$. The port voltage across R_{out} is given by $v_7^{(k)} = a_7^{(k-1)}/2$.

3) Global Scattering Stage: $\mathbf{a}^{(k)} = [a_1^{(k)}, \ldots, a_N^{(k)}]^T$ is computed, given $\mathbf{b}^{(k)} = [b_1^{(k)}, \ldots, b_N^{(k)}]^T$, by

$$\mathbf{a}^{(k)} = \mathbf{S}\mathbf{b}^{(k)} \ . \tag{23}$$

4) Convergence Check: local and global scattering stages are iteratively repeated until the following convergence condition is met, $\|\mathbf{a}^{(k)} - \mathbf{a}^{(k-1)}\|_2 < \varepsilon_{\text{SIM}}$, where ε_{SIM} is a small tolerance (e.g. 10^{-5}).

4.2 Convergence Analysis

In order to perform a convergence analysis of SIM applied to the ring modulator circuit, let us describe the nth (linear or nonlinear) circuit element with the general implicit function

$$f_n(v_n, i_n) = 0 \, . \tag{24}$$

At kth iteration of SIM, (24) can be linearized around the point with coordinates $v_n^{(k)}$ and $i_n^{(k)}$. The linearization corresponds to an instantaneous Thévenin equivalent circuit with equation

$$v_n^{(k)} - V_{\text{G}n}^{(k)} - R_{\text{G}n}^{(k)} i_n^{(k)} = 0 \ , \tag{25}$$

where $V_{\text{G}n}^{(k)}$ is the source of the Thévenin equivalent and $R_{\text{G}n}^{(k)}$ is its series resistance, defined as

$$R_{\text{G}n}^{(k)} = \frac{d}{di_n}\left[f_n\left(v_n^{(k)}, i_n^{(k)}\right)\right] = -\frac{\partial f_n\left(v_n^{(k)}, i_n^{(k)}\right)/\partial i_n}{\partial f_n\left(v_n^{(k)}, i_n^{(k)}\right)/\partial v_n} \, . \tag{26}$$

From (16), (22) and (25), we get the linearized WD scattering relation in matrix form

$$\mathbf{b}^{(k)} = \mathbf{D}^{(k)}\mathbf{a}^{(k-1)} + \mathbf{E}^{(k)}\mathbf{V}_{\text{G}}^{(k)} \ , \tag{27}$$

where $\mathbf{D}^{(k)} = \text{diag}[c_1^{(k)}, \ldots, c_N^{(k)}]^T$ and $\mathbf{E}^{(k)} = \text{diag}[e_1^{(k)}, \ldots, e_N^{(k)}]^T$ are diagonal matrices,

$$c_n^{(k)} = (R_{\text{G}n}^{(k)} - Z_n)/(R_{\text{G}n}^{(k)} + Z_n) \ , \tag{28}$$

$$e_n^{(k)} = 2Z_n/(R_{Gn}^{(k)} + Z_n) \ , \tag{29}$$

and $\mathbf{V}_{\mathrm{G}}^{(k)} = [V_{\mathrm{G1}}^{(k)}, \ldots, V_{\mathrm{GN}}^{(k)}]^T$. Plugging (23) in (27) and being $\mathbf{S}$ selfinverse, we get

$$\mathbf{a}^{(k)} = \mathbf{S}\mathbf{D}^{(k)}\mathbf{a}^{(k-1)} + \mathbf{S}\mathbf{E}^{(k)}\mathbf{V}_{\mathrm{G}}{}^{(k)} \ , \tag{30}$$

which shows how SIM can be interpreted as an iterative relaxation method with iteration matrices $\mathbf{S}\mathbf{D}^{(k)}$. It follows that a sufficient converge condition for SIM is

$$\rho\left(\prod_{k=1}^{K} \mathbf{S}\mathbf{D}^{(k)}\right) < 1 \ , \tag{31}$$

for any index $K \geq 1$, where $\rho\left(\prod_{k=1}^{K} \mathbf{S}\mathbf{D}^{(k)}\right) = \max\{|\lambda_1|, \ldots, |\lambda_N|\}$ is the spectral radius of matrix $\prod_{k=1}^{K} \mathbf{S}\mathbf{D}^{(k)}$ and λ_n with $1 \leq n \leq N$ is the nth eigenvalue of $\prod_{k=1}^{K} \mathbf{S}\mathbf{D}^{(k)}$.
Hereafter, a re-statement of the Theorem proved in [25], useful for the analysis of SIM, is reported.

Theorem 1: Let $\mathbf{S}$ be a $N \times N$ scattering matrix describing a reciprocal connection network and based on the voltage wave definition (2), and let $\left\{\mathbf{D}^{(1)}, \ldots, \mathbf{D}^{(K)}\right\}$ be a set of $K \geq 1$ diagonal matrices with dimensions $N \times N$. The following inequality always holds true

$$\rho\left(\prod_{k=1}^{K} \mathbf{S}\mathbf{D}^{(k)}\right) \leq \prod_{k=1}^{K} \rho\left(\mathbf{D}^{(k)}\right) \ , \tag{32}$$

where $\rho\left(\prod_{k=1}^{K} \mathbf{S}\mathbf{D}^{(k)}\right)$ and $\rho\left(\mathbf{D}^{(k)}\right)$ are the spectral radii of $\prod_{k=1}^{K} \mathbf{S}\mathbf{D}^{(k)}$ and $\mathbf{D}^{(k)}$, respectively.

The above re-statement of the Theorem in [25] highlights its validity, not only for scattering matrices describing simple "wire interconnections", but also, more in general, for scattering matrices describing arbitrary reciprocal connection networks embedding reciprocal multi-ports. It is worth noticing that, as the scattering matrix $\mathbf{S}$ describing an arbitrary reciprocal connection network satisfies all the properties of Table 1, the proof of Theorem 1 is the same as the one reported in [25]. In particular, it follows that Theorem 1 is applicable to the scattering matrix used for modeling the ring modulator connection network with multi-winding transformers, since, as shown in Subsection 2.2, it is reciprocal.
According to (32), if $\max\{|c_1^{(k)}|, \ldots, |c_N^{(k)}|\} < 1$ for each k, convergence of SIM is guaranteed, as $\rho\left(\mathbf{D}^{(k)}\right) = \max\{|c_1^{(k)}|, \ldots, |c_N^{(k)}|\}$ and the condition $\prod_{k=1}^{K} \rho\left(\mathbf{D}^{(k)}\right) < 1$ always holds true. Choosing positive free parameters, i.e. $Z_n > 0$, according to (28), condition $\max\{|c_1^{(k)}|, \ldots, |c_N^{(k)}|\} < 1$ reduces to

$$R_{Gn}^{(k)} > 0 \ . \tag{33}$$

In the following, we will show that condition (33) always holds in the case of the ring modulator circuit. In fact, the implicit derivative w.r.t. i of (20) is

$$\frac{d}{di}\left[f(v,i)\right] = \frac{1 + \frac{R_s}{R_p} + \frac{I_s R_s}{\eta V_t}\exp\left(\frac{v - R_s i}{\eta V_t}\right)}{\frac{1}{R_p} + \frac{I_s}{\eta V_t}\exp\left(\frac{v - R_s i}{\eta V_t}\right)} \ . \tag{34}$$

Being the parameters R_s, R_p, I_s, η and V_t positive, (34) is always positive; therefore, $R_{\mathrm{G1}}^{(k)} = \frac{d}{di}\left[f\left(v_1^{(k)}, i_1^{(k)}\right)\right]$, $R_{\mathrm{G2}}^{(k)} = \frac{d}{di}\left[f\left(v_2^{(k)}, i_2^{(k)}\right)\right]$, $R_{\mathrm{G3}}^{(k)} = \frac{d}{di}\left[f\left(v_3^{(k)}, i_3^{(k)}\right)\right]$ and $R_{\mathrm{G4}}^{(k)} = \frac{d}{di}\left[f\left(v_4^{(k)}, i_4^{(k)}\right)\right]$ are always positive. For the real generators and the resistor we have $R_{\mathrm{G5}}^{(k)} = R_{\mathrm{c}}$, $R_{\mathrm{G6}}^{(k)} = R_{\mathrm{in}}$ and $R_{\mathrm{G7}}^{(k)} = R_{\mathrm{out}}$; therefore, $R_{\mathrm{G5}}^{(k)}$, $R_{\mathrm{G6}}^{(k)}$ and $R_{\mathrm{G7}}^{(k)}$ are always positive. It follows that the convergence of SIM, applied to the ring modulator circuit, is theoretically guaranteed.
In the light of (30) and (31), we deduce that the converge speed of SIM strongly depends on the magnitude of the nonzero entries of $\mathbf{D}^{(k)}$. The closer Z_n is to $R_{Gn}^{(k)}$, the smaller the magnitude of the corresponding nonzero entry of $\mathbf{D}^{(k)}$. When the magnitude of the nonzero entries of $\mathbf{D}^{(k)}$ is reduced, also the spectral radius of the iteration matrices $\mathbf{S}\mathbf{D}^{(k)}$ is reduced and the convergence speed of SIM is increased. The ideal case is the one of full adaptation in which we are able to set $Z_n = R_{Gn}^{(k)}$ at each port n, the spectral radius of the iteration matrices reduces to zero and SIM converges in one iteration. As shown in Subsection 3.1, adaptation is easily performed when dealing with real voltage sources and resistors. Conversely, diodes cannot be adapted and the optimal value of the free parameter Z_n, which minimizes the corresponding reflection coefficient in matrix $\mathbf{D}^{(k)}$ changes according to the actual operating point. In particular, at each time step m, the optimal value for the nth free parameter would be $Z_n = \frac{d}{di}\left[f_n(v(m), i(m))\right]$, i.e. the implicit derivative (34) evaluated at the actual operating point with coordinates $v(m)$and $i(m)$. However, the actual operating point is unknown at the beginning of the mth time step; therefore, also the optimal value for

Z_n is unknown. For this reason, the adopted strategy is setting the parameters Z_1, Z_2, Z_3 and Z_4 equal to the implicit derivatives (34) evaluated at the operating points of the previous time step $m-1$.

5 Results

Results of the proposed WD implementation of the ring-modulator circuit, along with an accuracy analysis and efficiency analysis, are presented in this Section.
The input signal is a sampled sinusoid $V_{\text{in}}(m) = g_{\text{in}}\sin(2\pi f_{\text{in}} m/F_s)$, where m is the sampling step, F_s is the sampling frequency, g_{in} is the amplitude gain and f_{in} is the fundamental frequency.
Similarly, the carrier signal is a sampled sinusoid $V_{\text{c}}(m) = g_{\text{c}}\sin(2\pi f_c m/F_s)$, where g_{c} and f_c are its amplitude gain and fundamental frequency, respectively.
In all simulations, the sampling frequency is $F_s = 96$ kHz, amplitude gains are set to $g_{\text{in}} = g_{\text{c}} = 1$ V, series resistances are set to $R_{\text{in}} = R_{\text{c}} = 1\ \Omega$, while fundamental frequencies are specified case by case. The output resistance is always set to $R_{\text{out}} = 10\ \text{M}\Omega$, unless otherwise specified. The four diodes are identical and characterized by the same parameters. The following parameters of the extended Shockley diode model are fixed in all simulations; $V_t = 26$ mV, $I_s = 1$ pA and $\eta = 2.19$. As shown in Subsection 3.2, the extended Shockley diode model also contains the parameters R_s and R_p; the next Subsection discusses the importance of such parameters for the WD implementation of audio circuits with diodes based on SIM.

5.1 Motivation on the use of the Extended Shockley Diode Model

Although the use of resistances R_s and R_p is not only physically meaningful, but also very important for an accurate modeling of p-n junctions of diodes in many research fields [34], in the literature on the WD modeling of audio circuits, they are usually ignored and the traditional Shockley diode model without series and parallel resistances is employed; see, e.g., [7, 22, 24]. However, we have experimentally verified that the use of an unique one-port WD block implementing the extended Shockley diode model characterized by equation (20), is useful for preventing numerical problems that, instead, might arise when SIM is applied to the traditional Shockley diode model. In fact, at each time step SIM requires to set the port resistance Z_n equal to the slope of the tangent line passing through the operating point on the $v-i$ characteristic of the nth element at the previous time step. It follows that, dealing with the very high (e.g. $> 10^{20}$) or very low (e.g. $< 10^{-20}$) slopes of lines tangent to the $v-i$ curve of the traditional exponential Shockley diode model, numerical problems may arise. The adopted strategy to cope with this problem is to add a low series resistance R_s and a high parallel resistance R_p to the exponential diode model in order to limit the range of possible slopes on both the positive and the negative sides of the diode $v-i$ curve. In the following, we show that, when R_s is sufficiently low and R_p is sufficiently high, the aforementioned numerical problems are solved, with a negligible impact on the accuracy of the results. Two studies on how the parameters R_s and R_p affect the accuracy and the efficiency of the WD implementation of the ring modulator circuit based on SIM are presented in the following Subsection.

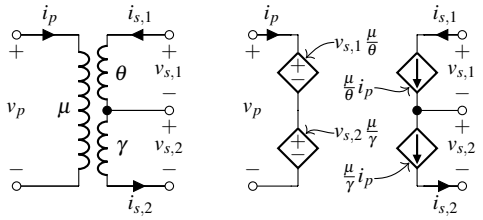

(a) Transformer. **(b)** Equivalent Circuit.

Fig. 4: An ideal 3-winding transformer and a possible realization using controlled sources.

5.2 Accuracy Analysis and Efficiency Analysis

Accuracy of the proposed WD implementation of the ring modulator circuit is studied comparing it with the corresponding implementation in a SPICE-like simulator (LTspice). In order to perform a fair comparison, a proper *instantaneous model*, i.e. an equivalent circuit with no reactive behavior, of the ideal 3-winding transformer should be used in LTspice. A possible model of the sort, based on a pair of current-controlled current sources and a pair of voltage-controlled voltage sources, is represented in Fig. 4.
In a ring modulator, when signals V_{in} and V_{c} are sinusoids, the actual frequency component of the carrier is highly attenuated in the output signal [6]. In particular, if one ratio among $f_{\text{c}}/f_{\text{in}}$ and $f_{\text{in}}/f_{\text{c}}$ is a rational number, the output signal will be harmonic, otherwise it will be inharmonic.

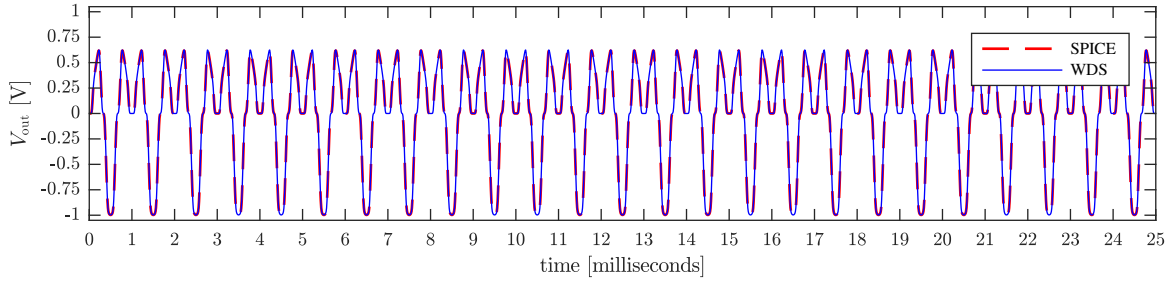

(a) Harmonic ring modulator output signal V_{out}.

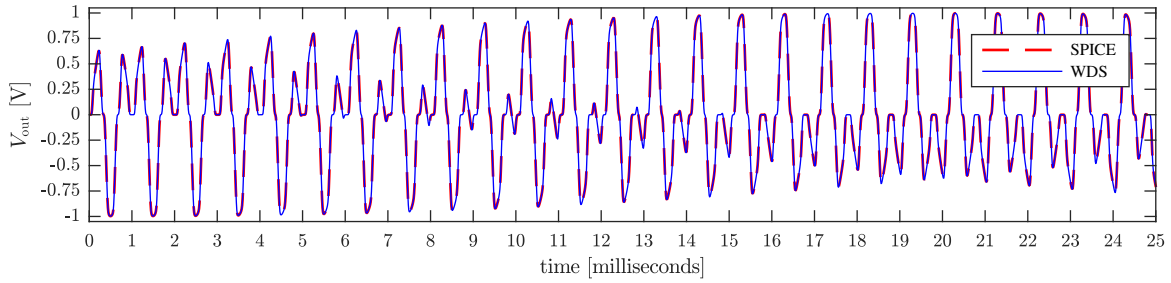

(b) Inharmonic ring modulator output signal V_{out}.

Fig. 5: Harmonic ($f_{\text{in}} = 500$ Hz, $f_{\text{c}} = 1500$ Hz) and inharmonic ($f_{\text{in}} = 505$ Hz, $f_{\text{c}} = 1490$ Hz) ring modulator output signals.

Fig. 5a shows a comparison of the periodic output signals V_{out} by LTspice and by the WD implementation running on a standard quad-core processor in the MATLAB environment, being $f_{\text{in}} = 500$ Hz, $f_{\text{c}} = 1500$ Hz and $f_{\text{c}}/f_{\text{in}} = 3$. $R_s = 10^{-2}$ Ω and $R_p = 10^{7}$ Ω, while in LTspice the series and shunt resistances of the p-n junctions are set to zero. The accuracy of the WD implementation is high, as *the average of the absolute value of the error* between its output signal and the one by LTspice, i.e. $|\bar{E}| = (1/M)\sum_{m=1}^{M} \left|V_{\text{out}}^{\text{WD}}(m) - V_{\text{out}}^{\text{SPICE}}(m)\right|$, where $M = 2400$ is the number of samples, is just $|\bar{E}| \simeq 6$ mV.

For measuring the computational cost of the WD implementation, $\Gamma = 1000$ simulations identical to the one already described are executed and *the real time ratio*, defined as RTR$= (1/\Gamma)\sum_{i=1}^{\Gamma}(t_{ei}/(M/F_s))$, where t_{ei} is the computational cost of the ith simulation in seconds, is computed. The lower the RTR, the better. We get RTR$\simeq 4.6$, which is lower than the RTR obtained applying the state-of-the-art WD algorithm described in [22] to the same circuit, i.e. RTR$\simeq 5.8$. However, it is worth noticing that dealing with the method in [22] the traditional Shockley diode model has been used, as, in that context, it did not cause numerical problems.

As an alternative example, Fig. 5b shows a comparison of the aperiodic output signals V_{out} by LTspice and by the corresponding WD implementation in the case in which $f_{\text{in}} = 505$ Hz, $f_{\text{c}} = 1490$ Hz and $f_{\text{c}}/f_{\text{in}} \simeq 2.95$, $R_s = 10^{-2}$ Ω and $R_p = 10^{7}$ Ω; accuracy and efficiency performances of the WD implementation are similar to those of the previous example.

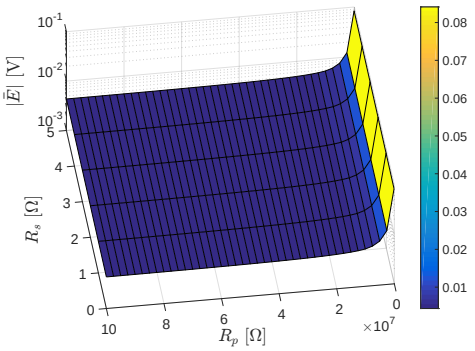

Fig. 6: $|\bar{E}|$ as a function of R_s and R_p.

The 3D plot in Fig. 6 shows how $|\bar{E}|$ is affected by the variation of $R_s \in [10^{-3}, 5]$ Ω and $R_p \in [10^{5}, 10^{8}]$ Ω. We observe that, for the considered configuration of signals and parameters, $|\bar{E}|$ depends more on R_p than on R_s. Moreover, $|\bar{E}|$ is almost constant for R_p

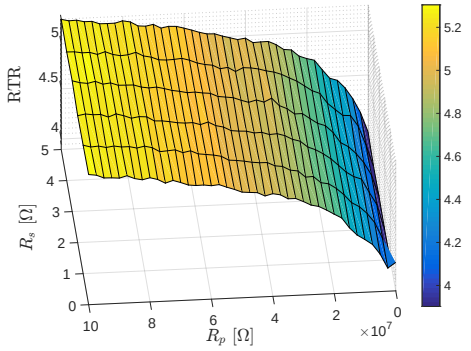

Fig. 7: RTR as a function of R_s and R_p.

ranging from 10^6 to 10^8 Ω, increasing very slowly for values lower than $R_p \simeq 10^6$ and exhibiting a sharper increase for higher values of R_p. Similarly, the 3D plot in Fig. 7 shows how RTR is affected by the variation of $R_s \in [10^{-3}, 5]$ Ω and $R_p \in [10^5, 10^8]$ Ω. We notice that also RTR depends more on R_p than on R_s. In general, RTR is lower for lower values of R_p and for higher values of R_s.

6 Discussion

The results of the proposed WD implementation of the ring modulator based on SIM, along with the discussion on the results presented in [25], confirm that the adopted approach is suitable for Virtual Analog modeling of audio circuits with one-port nonlinearities characterized by monotonic $v-i$ curves, e.g. diodes. Here follow some properties of the proposed method that are desirable in Virtual Analog applications.

1) Guarantee of convergence: convergence of SIM is theoretically guaranteed if the linear or nonlinear one-port circuit elements are characterized by monotonic $v-i$ curve, as in the case of the ring modulator. Numerical problems that might arise are avoided using the strategy discussed in Subsection 5.1. Conversely, it is worth noticing that convergence of state-of-the-art WD methods [22], based on multi-dimensional NR solvers, whose dimensionality equals the total number of ports of the nonlinear elements, is not guaranteed.

2) Accuracy: as shown in Subsection 5.1, the achieved accuracy is high. When R_s is low and R_p is high their impact on accuracy is negligible. The achieved accuracy is comparable to the one of state-of-the-art WD algorithms [22]. The only difference is that the method in [22] does not require the use of an extended Shockley diode model, since, at least in the performed simulations, numerical problems do not arise employing the traditional Shockley diode model.

3) Efficiency: as shown in Subsection 5.1, the computational cost of the proposed method is comparable to the one of state-of-the-art WD algorithms [22] or even less. Moreover, it is worth noticing that the ring modulator circuit is a very small circuit. In fact, it has been shown in [25] that the efficiency gain with respect to implementations based on multi-dimensional NR solvers can be far higher, dealing with larger nonlinear circuits.

4) Parallelizability: local scattering stage of SIM is *embarrassingly parallelizable*, hence each one-dimensional NR solver can potentially run on a separate thread of execution. Again, this property becomes more and more important as we are dealing with larger nonlinear circuits. In this paper, as the ring modulator is a small circuit, parallelizability has not been exploited. It is worth noticing that WD algorithms based on multi-dimensional NR solvers [22] are not parallelizable.

5) Intrinsic ability of accommodating time-varying parameters: since SIM already requires the update of the port resistances and the scattering matrix at each time-step, it can naturally handle time-varying parameters, e.g. the port resistance which is set equal to the output resistor or the turn-ratios of the multi-winding transformers, without complicating the computational flow. For this reason, a WD implementation based on SIM of a time-varying version of the ring modulator circuit does not require a significant increase of the computational cost w.r.t. the implementation of a static version. Conversely, the WD implementation of time-varying circuits with state-of-the art algorithms would require to recompute the scattering matrix and the used conversion matrices [22] at each time-step (operations which are performed once in the static case). In the light of this, even though we are not going to show quantitative comparisons, since systematic experiments have not been performed, we verified that the efficiency gain in using SIM w.r.t. state-of-the-art WD algorithm is even higher, when dealing with time-varying circuits.

7 Summary

In this paper, we presented a robust, accurate and efficient WD implementation of the ring modulator circuit, which proved to be a suitable case study for developing recent advances in the theory on WD structures [25]. Firstly, we showed how WD scattering matrices which describe connection networks embedding

multi-winding transformers can be efficiently implemented. Secondly, we showed how the Scattering Iterative Method, already developed for the analysis of large nonlinear photovoltaic arrays, can be successfully adopted for the time-domain emulation of circuits containing multiple diodes in Virtual Analog applications. Future research will be devoted to the extension of the Scattering Iterative Method to dynamic circuits and circuits with multi-port nonlinearities.

References

[1] Cowan, F. A., "Modulating System," 1935, U.S. Patent # 2,025,158, Filed 7 June 1934, Issued 24 Dec. 1935.

[2] Bode, H., "History of Electronic Sound Modification," *J. Audio Eng. Soc.*, 32(10), pp. 730–739, 1984.

[3] Oberheim, T. E., "A "Ring Modulator" Device for the Performing Musician," in *Proc. Audio Eng. Soc. 38th Conv.*, 1970.

[4] Parker, J., "A simple digital model of the diode-based ring-modulator," in *Proc. 14th Int. Conf. Digital Audio Effects*, pp. 163–166, Paris, France, 2011.

[5] Hoffmann-Burchardi, R., "Digital simulation of the diode ring modulator for musical applications," in *Proc. 11th Int. Conf. Digital Audio Effects*, pp. 165–168, Espoo, Finland, 2008.

[6] Hoffmann-Burchardi, R., "Asymmetries make the difference: An analysis of transistor-based analog ring modulators," in *Proc. 12th Int. Conf. Digital Audio Effects*, Como, Italy, 2009.

[7] Bernardini, A., Werner, K. J., Sarti, A., and Smith, J. O., "Modeling Nonlinear Wave Digital Elements using the Lambert Function," *IEEE Trans. Circuits and Systems I: Regular Papers*, 63, pp. 1231–1242, 2016.

[8] Bilbao, S., *Wave and Scattering Methods for Numerical Simulation*, John Wiley & Sons, New York, first edition, 2004.

[9] De Sanctis, G. and Sarti, A., "Virtual analog modeling in the wave-digital domain," *IEEE Transactions on Audio, Speech and Language Processing*, 18(4), pp. 715–727, 2010.

[10] Bernardini, A., Antonacci, F., and Sarti, A., "Wave Digital Implementation of Robust First-Order Differential Microphone Arrays," *IEEE Signal Process. Lett.*, 25(2), pp. 253–257, 2018.

[11] Werner, K. J., Smith, J. O., and Abel, J. S., "Wave Digital Filter Adaptors for Arbitrary Topologies and Multiport Linear Elements," in *Proc. 18th Int. Conf. Digital Audio Effects*, pp. 379–386, Trondheim, Norway, 2015.

[12] Werner, K. J., Nangia, V., Smith, J. O., and Abel, J. S., "Resolving Wave Digital Filters with Multiple/Multiport Nonlinearities," in *Proc. 18th Int. Conf. Digital Audio Effects*, pp. 387–394, Trondheim, Norway, 2015.

[13] Verasani, M., Bernardini, A., and Sarti, A., "Modeling Sallen-Key audio filters in the Wave Digital domain," in *Proc. IEEE Int. Conf. Acoustics, Speech and Signal Processing (ICASSP)*, pp. 431–435, 2017.

[14] Paiva, R. C. D., D'Angelo, S., Pakarinen, J., and Välimäki, V., "Emulation of operational amplifiers and diodes in audio distortion circuits," *IEEE Trans. Circuits Syst. II, Exp. Briefs*, 59, pp. 688–692, 2012.

[15] Bernardini, A., Werner, K. J., Sarti, A., and Smith, J. O., "Multi-Port NonLinearities in Wave Digital Structures," in *Proc. IEEE Int. Symp. Signals Circuits Syst.*, Iași, Romania, 2015.

[16] Bernardini, A., Werner, K. J., Sarti, A., and Smith, J. O., "Modeling a class of multi-port nonlinearities in wave digital structures," in *Proc. 23rd European Signal Process. Conf.*, pp. 669–673, Nice, France, 2015.

[17] Schwerdtfeger, T. and Kummert, A., "Newton's method for modularity-preserving multidimensional wave digital filters," in *IEEE 9th Int. Workshop on Multidimensional (nD) Systems (nDS)*, Vila Real, Portugal, 2015.

[18] Werner, K. J., Nangia, V., Bernardini, A., Smith, J. O., and Sarti, A., "An Improved and Generalized Diode Clipper Model for Wave Digital Filters," in *Proc. Conv. Audio Eng. Soc.*, New York, NY, 2015.

[19] Bernardini, A. and Sarti, A., "Dynamic Adaptation of Instantaneous Nonlinear Bipoles in Wave Digital Networks," in *Proc. 24th European Signal Process. Conf.*, Budapest, Hungary, 2016.

[20] Bernardini, A. and Sarti, A., "Canonical piecewise-linear representation of curves in the wave digital domain," in *Proc. 25th European Signal Process. Conf.*, pp. 1125–1129, Kos, Greece, 2017.

[21] Bernardini, A. and Sarti, A., "Biparametric Wave Digital Filters," *IEEE Transactions on Circuits and Systems I: Regular Papers*, 64(7), pp. 1826–1838, 2017.

[22] Olsen, M. J., Werner, K. J., and Smith, J. O., "Resolving Grouped Nonlinearities in Wave Digital Filters Using Iterative Techniques," in *Proc. 19th Int. Conf. Digital Audio Effects*, pp. 279–286, Brno, Czech Republic, 2016.

[23] Werner, K. J., Olsen, M. J., Rest, M., and Parker, J. D., "Generalizing Root Variable Choice in Wave Digital Filters with Grouped Nonlinearities," in *Proc. 20th Int. Conf. Digital Audio Effects*, pp. 176–183, Edinburgh, UK, 2017.

[24] Rest, M., Parker, J. D., and Werner, K. J., "WDF Modeling of a Korg MS-50 based non-linear diode bridge VCF," in *Proc. 20th Int. Conf. Digital Audio Effects*, pp. 145–151, Edinburgh, UK, 2017.

[25] Bernardini, A., Maffezzoni, P., Daniel, L., and Sarti, A., "Wave-Based Analysis of Large Nonlinear Photovoltaic Arrays," *IEEE Transactions on Circuits and Systems I: Regular Papers*, 65(4), pp. 1363–1376, 2018.

[26] Bernardini, A., Sarti, A., Maffezzoni, P., and Daniel, L., "Wave Digital-Based Variability Analysis of Electrical Mismatch in Photovoltaic Arrays," in *Proc. IEEE International Symposium on Circuits and Systems (ISCAS)*, Florence, Italy, 2018.

[27] Martens, G. O. and Meerkötter, K., "On N-port adaptors for wave digital filters with application to a bridged-tee filter," in *Proc. IEEE Int. Symp. Circuits Syst.*, p. 514–517, Munich, Germany, 1976.

[28] Martens, G. O. and Lê, H. H., "Wave digital adapters for reciprocal second-order sections," *IEEE Transactions on Circuits and Systems*, 25(12), pp. 1077–1083, 1978.

[29] Jarmasz, M. and Martens, G. O., "Design of canonic wave digital filters using Brune and matched 4-port adaptors," *IEEE Trans. on Circuits and Systems*, 34(5), pp. 480–495, 1987.

[30] Meerkötter, K. and Fränken, D., "Digital Realization of Connection Networks by Voltage-Wave 2-port Adapters," *AEU - Int. J. of Electronics and Commun.*, 50(6), pp. 362–367, 1996.

[31] Fränken, D., Ochs, J., and Ochs, K., "Generation of wave digital structures for connection networks containing multiport elements," *IEEE Trans. Circuits and Systems I: Regular Papers*, 52, pp. 586–596, 2005.

[32] Chua, L., Desoer, C., and Kuh, E., *Linear and Nonlinear Circuits*, Circuits and systems, McGraw-Hill, 1987.

[33] Fettweis, A., "Wave digital filters: Theory and practice," *Proceedings of the IEEE*, 74(2), pp. 270–327, 1986.

[34] Ortiz-Conde, A., Garcia-Sánchez, F. J., Muci, J., and Sucre-González, A., "A review of diode and solar cell equivalent circuit model lumped parameter extraction," *Facta Universitatis, Series: Electronics and Energetics*, 27, pp. 57–102, 2014.